Deep-Sea Research I 83 (2014) 93–101

Contents lists available at ScienceDirect

Deep-Sea Research I

journal homepage: www.elsevier.com/locate/dsri

Seasonal dynamics in colored dissolved organic matter in the Mediterranean Sea: Patterns and drivers

Xiaogang Xing [a,b], Hervé Claustre [c,d], Haili Wang [b,*], Antoine Poteau [c,d], Fabrizio D'Ortenzio [c,d]

[a] Key Laboratory of Physical Oceanography, Ocean University of China, Ministry of Education, Qingdao, China
[b] State Key Laboratory of Marine Environmental Science, Xiamen University, Xiamen, China
[c] Université Pierre et Marie Curie (Paris-6), UnitéMixte de Recherche 7093, Laboratoired'Océanographie de Villefranche, Villefranche-sur-Mer, France
[d] Centre National de la RechercheScientifique, UnitéMixte de Recherche 7093, Laboratoired'Océanographie de Villefranche, Villefranche-sur-Mer, France

ARTICLE INFO

Article history:
Received 19 July 2013
Received in revised form
19 September 2013
Accepted 21 September 2013
Available online 8 October 2013

Keywords:
Dissolved organic matter
Phytoplankton
Drifters
Biogeochemistry
Optics

ABSTRACT

Two autonomous profiling "Bio-Argo" floats were deployed in the northwestern and eastern sub-basins of the Mediterranean Sea in 2008. They recorded at high vertical (1 m) and temporal (5 day) resolution, the vertical distribution and seasonal variation of colored dissolved organic matter (CDOM), as well as of chlorophyll-a concentration and hydrological variables. The CDOM standing stock presented a clear seasonal dynamics with the progressive summer formation and winter destruction of subsurface CDOM maxima (YSM, for Yellow Substance Maximum). It was argued that subsurface CDOM is a by-product of phytoplankton, based on two main characteristics, (1) the YSM was located at the same depth than the deep chlorophyll maximum (DCM) and (2) the CDOM increased in summer parallels the decline in chlorophyll-a. These observations suggested an indirect but tight coupling between subsurface CDOM and phytoplankton via microbial activity or planktonic foodweb interactions. Moreover, the surface CDOM variations observed both by floats and MODIS displayed different seasonal dynamics from what recorded at subsurface one. This implies that CDOM standing stock can be hardly detected by satellite. It is worthnoting that surface CDOM was found to be more related to the sea surface temperature (SST) than chlorophyll-a concentration, suggesting its physical origin, in contrast to the biological origin of YSM and subsurface standing stocks.

© 2013 Published by Elsevier Ltd.

1. Introduction

Colored (or Chromophoric) Dissolved Organic Matter (abbreviated as "CDOM"), also known as "gelbstoff" (Kalle, 1938), "yellow substance" (Shifrin, 1988), or "gilvin" (Kirk, 1994), is an important component of the dissolved organic carbon (DOC) pool in natural waters where it plays a major role in determining underwater light availability (Siegel et al., 1995, 2002; Siegel and Michaels, 1996; Nelson et al., 1998; Nelson and Siegel, 2002; Coble, 2007; Morel and Gentili, 2009a).

The main optical behavior of CDOM resides in its light absorption over a broad range of visible and UV wavelengths. Especially in the UV and blue light region, the non-water absorption is dominated by CDOM (Nelson and Siegel, 2002). Statistical analysis using global satellite data shows that nearly 50% of non-water absorption is due to CDOM at 440 nm, which also corresponds to the main phytoplankton absorption peak (Swan et al., 2009). Thus, CDOM can affect on the accuracy of the retrieval of ocean chlorophyll-a concentration and subsequently primary productivity by satellite ocean color radiometry.

However, due to severe under-sampling through the use of ship-based observation, in situ measurements have remained scarce and hence our understanding of CDOM dynamics in various open ocean regions. In this context, the CDOM time series (based on monthly cruises) at BATS and analyzed by Nelson et al. (1998) can be considered as a reference study for open ocean waters. More recently, the availability of new sensors (such as in situ CDOM fluorometers, Belzile et al., 2006; Kowalczuk et al., 2010) associated with the progressive maturation of autonomous platforms that can carry them (e.g. Johnson et al., 2009), might be of considerable importance in view of improving our understanding of CDOM dynamics by increasing temporal as well spatial resolution of measurements.

The fluorescent properties of CDOM have been reported as early as 1949 by Kalle (1949) who found that the same material was able to emit blue fluorescence when excited by UV radiations. Although relationships between CDOM absorption and fluorescence do not seem to be ubiquitous, nevertheless, linear relationships between both measurements were observed

* Corresponding author.
E-mail address: hwang@xmu.edu.cn (H. Wang).

0967-0637/$ - see front matter © 2013 Published by Elsevier Ltd.
http://dx.doi.org/10.1016/j.dsr.2013.09.008

in open oceans and coastal waters (e.g., Ferrari and Tassan, 1991; Hoge et al., 1993; Vodacek et al., 1997; Ferrari and Dowell, 1998; Ferrari, 2000; Belzile et al., 2006; Yamashita and Tanoue, 2009; Kowalczuk et al., 2010).

The recent development of the so-called Bio-Argo floats (profiling floats equipped with bio-optical and biogeochemical sensors) now offers the possibility to develop innovative strategies for the observation of oceanic biogeochemistry and ecosystem (Claustre et al., 2010). Bio-Argo floats not only allow for long-term (annual/multiyear), quasi-continuous (at least once per 10 days), and highly resolved vertical (1 m resolution) oceanic properties observations, but also provides unique, synchronous and multi-parameter datasets. Such datasets are especially required for physical and biological/biogeochemical/bio-optical coupling research (IOCCG, 2011).

In 2008, a fleet of 8 Bio-Argo floats were deployed in various oceanic areas representative of the diversity of the trophic conditions prevailing in the open ocean, equipped with CDOM fluorometer, chlorophyll-a fluorometer, as well as other bio-optical and biogeochemical sensors. The acquired dataset by this fleet supported methodological development allowing the accurate retrieval of key biogeochemical variables like chlorophyll-a concentration (Xing et al., 2011) and CDOM absorption at 412 nm (Xing et al., 2012). Two of these 8 floats were deployed in the northwestern and eastern sub-basins of the Mediterranean Sea and continuously recorded, over more than 1 year, the vertical distributions (from surface to 400 m) of CDOM as well as hydrological parameters and chlorophyll-a concentration. Here these high-resolution measurements are used as the basis for an assessment of the regional and seasonal CDOM dynamics.

The present study highlights the seasonal cycle of CDOM in both sub-basins, the decoupling between its surface and subsurface dynamics, and the tight link between its subsurface maximum and deep chlorophyll-a maximum (DCM). A specific attention is dedicated to the yellow substance subsurface maximum (hereafter denoted as YSM), a feature already investigated in Case I waters (e.g. Nelson et al., 1998, 2004; Coble et al., 1998; Chen, 1999; Lund-Hansen et al., 2006; Kitidis et al., 2006; Chekalyuk et al., 2012), and also reported in the Mediterranean Sea (Oubelkheir et al., 2005, 2007). Here in the Mediterranean Sea and thanks to the first complete high-resolution time series, the temporal CDOM dynamics and associated drivers can be addressed for the first time. In particular, the possible biogeochemical and/or the hydrological origins of the observed variations are presented and discussed.

2. Materials and methods

2.1. Bio-Argo data

The two Bio-Argo floats were deployed in May 2008, in the Northwestern Mediterranean Sea (NWM), and in June 2008, in the Levantine Sea (LS) (Fig. 1). They are named "MED_NW_B02" and "MED_LV_B06", respectively. Both floats are based on the PROVOR CTS3 free-drifting profilers (NKE instrumentation, France), equipped with a OC4 radiometer (Satlantic, Halifax, Canada), a transmissometer and an ECO Puck instrument (WET Labs, Inc., Philomath, OR, USA). In addition to the standard hydrological observation by PROVOR, the OC4 radiometer measures the downward planar irradiance, E_d, at three wavelengths (412, 490, and 550 nm); the transmissometer measures the beam attenuation coefficient at 660 nm; and the ECO Puck integrates three independent sensors, for backscattering at 532 nm, Chla fluorescence, and CDOM fluorescence (excitation at 370 nm, emission at 460 nm) measurements, respectively. The observation frequency was generally programmed as a profile every 5 days, with few exception of a profile every 1 day just after the deployment (to check float performances). For each profile, the observation mission included acquisition of a CTD profile from 1000 m up to surface, whereas the bio-optical sensors started acquisition from 400 m (this was done to save energy and hence increase the life-time of float).

In previous studies (Xing et al., 2011, 2012), two successive processing procedures were presented respectively for retrieval of chlorophyll-a concentration (units mg m^{-3}, thereafter denoted [Chla]) and CDOM absorption coefficient at 412 nm (units m^{-1}, thereafter denoted $a_y(412)$), combining the radiometry ($E_d(412)$ and $E_d(490)$) and fluorometry (chlorophyll and CDOM fluorescence). For the sake of completion, the retrieval methods are briefly introduced here.

First of all, two linear relationships were assumed as the basis of procedures, as shown below:

$$[\text{Chla}] = \text{Slope}_C(\text{Fluo}_C - \text{Offset}_C) \quad (1)$$

$$a_y(412) = \text{Slope}_Y(\text{Fluo}_Y - \text{Offset}_Y) \quad (2)$$

where [Chla] and $a_y(412)$ are the finally retrieved variables; Fluo_C and Fluo_Y represent the chlorophyll and CDOM fluorescence signals acquired by two fluorometers; and all the remaining terms (Slope_C, Slope_Y, Offset_C and Offset_Y) are regarded as the coefficients to be retrieved.

The Offset_C is determined profile by profile firstly based on a common assumption that the [Chla] at depths larger than 300 m is zero, so that the Fluo_C profiles are simply reset to zero beyond this level and the Offset_C are obtained as the deep Fluo_C signal. In light of the classical bio-optical relationship prevailing for open ocean Case I waters (Morel et al., 2007), the diffuse attenuation coefficient at 490 nm (thereafter denoted $K_d(490)$) can be calculated as a function of [Chla]:

$$K_d(490) = 0.01660 + 0.0825[\text{Chla}]^{0.6529} \quad (3)$$

By introducing Eq. (1) into Eq. (3), the Slope_C will be figured out while $K_d(490)$ is determined through the vertical derivation

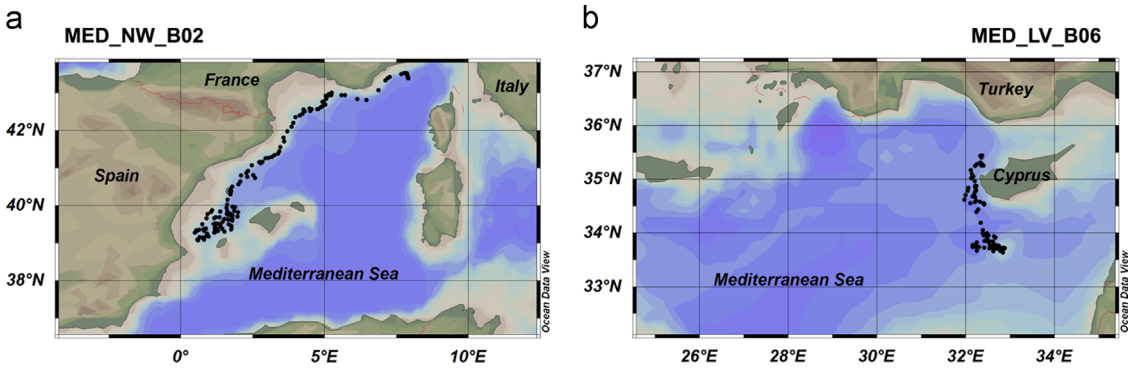

Fig. 1. The trajectories and observation positions of the "MED_NW_B02" float (a) in the northwestern sub-basin of Mediterranean Sea and the "MED_LV_B06" float (b) in the eastern sub-basin.

$E_d(490)$, according to the definition of diffuse attenuation (Xing et al., 2011).

The influence of CDOM on the diffuse attenuation coefficient is considerably more pronounced at 412 nm than at 490 nm, owing to the exponential increase in its absorption toward shorter wavelengths; therefore the $K_d(412)$ was better adapted to retrieve information on the CDOM content. Based on bio-optical relationships, a new empirical equation was established as follows:

$$K_d(412) = 0.01 + 0.0676[\mathrm{Chla}]^{0.686} + 1.3a_y(412) \quad (4)$$

Here, the three terms on the right side of Eq. (4) represent the respective contributions of pure seawater, particles and CDOM to the attenuation coefficient $K_d(412)$. From Eq. (4), once [Chla] has been retrieved (through Eq. (3)) and deriving $K_d(412)$ from $E_d(412)$, the CDOM absorption $a_y(412)$ can be subsequently derived. Thereafter, the corresponding coefficients ($\mathrm{Slope_Y}$ and $\mathrm{Offset_Y}$) were determined via linear regression analysis between radiometry-based $a_y(412)$ and concurrently observed $\mathrm{Fluo_Y}$ profiles (Xing et al., 2012).

2.2. Satellite data

MODIS-Aqua remotely-sensed data (Level 3, 8-day composites, 9 km × 9 km resolution) are used to characterize the surface CDOM and its relationships with phytoplankton and temperature in larger regions than the area explored by floats. The surface [Chla] and CDOM absorption were retrieved from the evaluation products in MODerate resolution Imaging Spectroradiometer (MODIS) dataset based on the GSM ocean color model (Maritorena et al., 2002) provided by National Aeronautics and Space Administration (NASA). Actually, the GSM product is not strictly CDOM but $a_{dg}(443)$ which is the absorption coefficient at 443 nm by the colored detrital material (CDM), including the particulate detritus and dissolved CDOM. $a_{dg}(443)$ remains nevertheless essentially dominated by the contribution of dissolved material (Coble, 2007) and is here considered as a CDOM proxy. Additionally, the sea surface temperature (SST, 11 μm daytime) data were also retrieved. The average surface [Chla], $a_{dg}(443)$ and SST are calculated every 8 days in two regions, the whole Northwestern sub-basin (0–10°E, 39–45°N) and the Eastern sub-basin (30–37°E, 30–37°N), which encompass the float tracks and give a more regional picture of the observed trends.

2.3. Derived data

The mixed layer depth (MLD) is determined as the first depth where the density value is 0.03 kg m^{-3} in excess with respect to the value at 10 m De Boyer-Montegut et al. (2004).

In addition, two optically derived depths, the penetration depth (z_{pd}) and euphotic depth (z_{eu}), are derived from the [Chla] profile and empirical relationships. Firstly, $K_d(490)$ profile is determined from [Chla] via Eq. (3). Secondly, the attenuation coefficient for Photosynthetically Active Radiation (PAR), $K_d(PAR)$ is estimated from (Morel et al., 2007)

$$K_d(PAR) = 0.00665 + 0.874K_d(490) - 0.00121K_d(490)^{-1} \quad (5)$$

Then, the z_{pd} and z_{eu} are determined based on their own definitions:

$$\int_0^{z_{pd}} K_d(PAR, z)dz = 1 \quad (6)$$

$$\int_0^{z_{eu}} K_d(PAR, z)dz = 4.6 \quad (7)$$

3. Results and discussions

3.1. Hydrological context

Fig. 2a, b, d and e shows the time series in temperature and salinity distributions (0–400 m) acquired in both sub-basins. The black line on each panel represents the 28.88 isopycnal (on which, the water density equals to 1028.88 kg m^{-3}), selected to highlighting specific features in deep CDOM, especially in the eastern sub-basin (see Section 3.3).

In the NWM, float MED_NW_B02 was deployed off the coast of Nice in May, 2008. During its nearly 2-year life-time period, it drifted toward southwest together with the Liguro-Provenco-Catalan Current (Herbaut et al., 1996; Fusco et al., 2003), passed through the Gulf of Lion transiently, and then stayed in the Balearic Sea (Fig. 1a). The surface temperature varied over a wide range from 13 °C in winter to 28 °C in summer. From ~100 to 1000 m (the profiles from 400 to 1000 m are not shown), the temperature largely did not vary seasonally (~13 °C) (Fig. 2a). As for the salinity, the values ranged from 37.8 to 38.2 at surface and increased with depth; however, there existed a water mass with high salinity always below ~50 m (Fig. 2b).

The float (MED_LV_B06) deployed in the eastern sub-basin (south of Cyprus) stayed around 9 months south of 34°N within an anticyclonic gyre. The stability hydrological patterns suggested that this 9-month time series can be analyzed as the seasonal evolution of the same water mass. Thereafter, the float drifted northward and stayed off the west coast of Cyprus (Fig. 1b). Correspondingly, the discrepancy of hydrological parameters can be seen obviously, away from the seasonal cycles at surface (Fig. 2d and e). During the first 9 months, the relatively stable dynamic of the gyre, induced very few variation of the physical characteristics of the water column as observed by the float. Only the surface layers exhibited an important seasonal variability, influenced by the atmospheric forcing and by the eastward flow of the Modified Atlantic Water (MAW). While after moving northward, this float recorded a low temperature low salinity water mass occupying the thermocline below 200 m up to 1000 m.

Apart from the data acquired in the eastern sub-basin after March, 2009, the hydrological environments in the upper layer (from surface to 400 m) between both sub-basins revealed quite marked disparities, concerning the summer surface maximum temperature (reaching up to 30 °C in the LS) as well as their vertical distribution. However, it declined with depth up to a relatively constant temperature (~17.5 °C) below 100 m, where the temperature was much colder (~13 °C) in the NWM.

3.2. CDOM distributions

The vertical distributions of retrieved CDOM absorption coefficient at 412 nm, $a_y(412)$ (Fig. 2c and f) has already been presented in the methodology-oriented paper of Xing et al. (2012). These results are here presented again as a preliminary step in view of understanding the CDOM dynamics in both Mediterranean environments.

In both sub-basins, CDOM profiles displayed a large seasonality, which can be summarized by a strong surface photobleaching in summer time, a high mixing in winter, and a seasonal subsurface enhancement. In summer, owing to exposure to intense sunlight, surface CDOM lost its absorptivity and fluorescence efficiency remarkably. Consequently, the minimum of $a_y(412)$ (less than 0.005 m^{-1}) always appeared at surface in summer. Another reason leading to the seasonality of surface CDOM was the strong mixing effect in winter, which not only generated a very deep homogenous CDOM layer that even may exceed 350 m in the eastern sub-basin, but also brought some deep CDOM into the upper layer. Besides, from summer to winter,

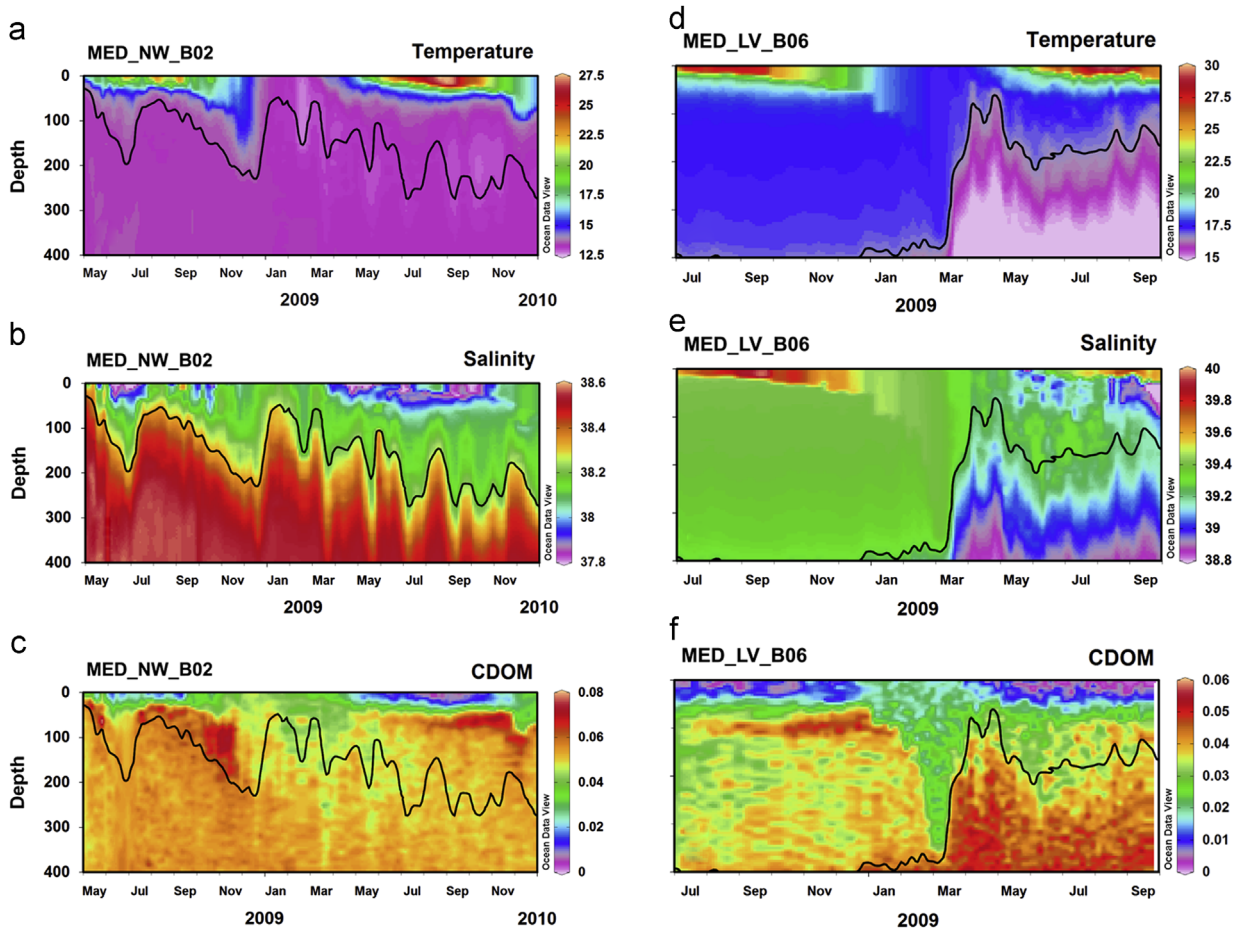

Fig. 2. The time series of temperature (units °C) (panels a and d), salinity (units psu) (panels b and e) and CDOM absorption coefficient ($a_y(412)$, units m^{-1}) (panels c and f) observed in the northwestern and eastern basin. The contour line on each panel represents the 28.88 isopycnal (the density equals to 1028.88 mg m^{-3}).

the CDOM profile was characterized by a subsurface maximum (YSM) which, was located around 100 m. In the northwestern sub-basin, the YSM started to develop in May, enhanced gradually up to November, and finally disappeared due to the physical mixing in mid-winter. Probably due to the influence of deep CDOM or to the difference of water mass with peculiar phytoplankton species composition, no obvious YSM was identified after June 2009 in the LS.

In addition to the seasonal patterns, a hydrology-related change of CDOM was recorded by the float MED_LV_B06 (Fig. 2f). As mentioned above, after the float escaping northward from the gyre, and the corresponding CDOM absorption increased markedly ($a_y(412) > 0.04\ m^{-1}$) at depth, which suggested that enhanced CDOM was a signature of specific water mass. The 28.88 isopycnal (black line), clearly delineated this signature (Fig. 2). Obviously, the CDOM below this isopycnal was elevated in the LS, but did not vary in the NWM.

3.3. Deep CDOM driven by hydrology

The scatter plots of $a_y(412)$ versus salinity and temperature are shown in Fig. 3 to examine the relationships between CDOM and hydrography, especially in the deep waters. The data below the 28.88 isopycnal are reported in black, the others in gray.

Overall, in the whole upper layer (for all points in Fig. 3), CDOM is negatively related to temperature in both sub-basins (especially at surface in Fig. 6). By contrast, there is no simply consistent relationship found between CDOM and salinity. However, in the deep waters (below 28.88 isopycnal), CDOM became more tightly related to temperature and salinity in the LS (Fig. 3c and d), with relatively high determination coefficients ($r^2 = 0.506$ and 0.474). In contrast, no clear relationships are found between deep CDOM and corresponding salinity or temperature ($r^2 = 0.123$ and 0.334) in the NWM, even if CDOM might appear positively related to the temperature (over a weak range). This discrepancy between both sub-basins indicates that the deep CDOM is controlled by water mass dynamics.

Actually, in most coastal areas and below the euphotic zone elsewhere in the open ocean, CDOM displays conservative behavior on the time scale of physical mixing. Monitoring CDOM fluorescence has often been used to distinguish between water masses from various sources (Mopper and Schultz, 1993; Coble, 1996), and study the mixing processes in coastal and estuarine waters (Laane and Kramer, 1990; De Souza Sierra et al., 1997). Moreover, deep CDOM in relation to water mass has been reported in many other oceanic regions. In the Gulf Stream, Chen and Bada (1992) found that patterns of CDOM fluorescence were in agreement with the distribution of water masses. In the Arabian Sea, Coble et al. (1998) presented that the high salinity high temperature Persian Gulf Water (PGW) contains more CDOM than adjacent waters, located at depth between 180 and 320 m. More recently, Nelson et al. (2007) and Swan et al. (2009) investigated the hydrographic controls on CDOM in the North Atlantic and Pacific, respectively. They concluded that CDOM distribution reflected the rapid advection and mixing processes within the basin, which supported the potential use of CDOM as a tracer of ocean circulation processes for subducted water masses.

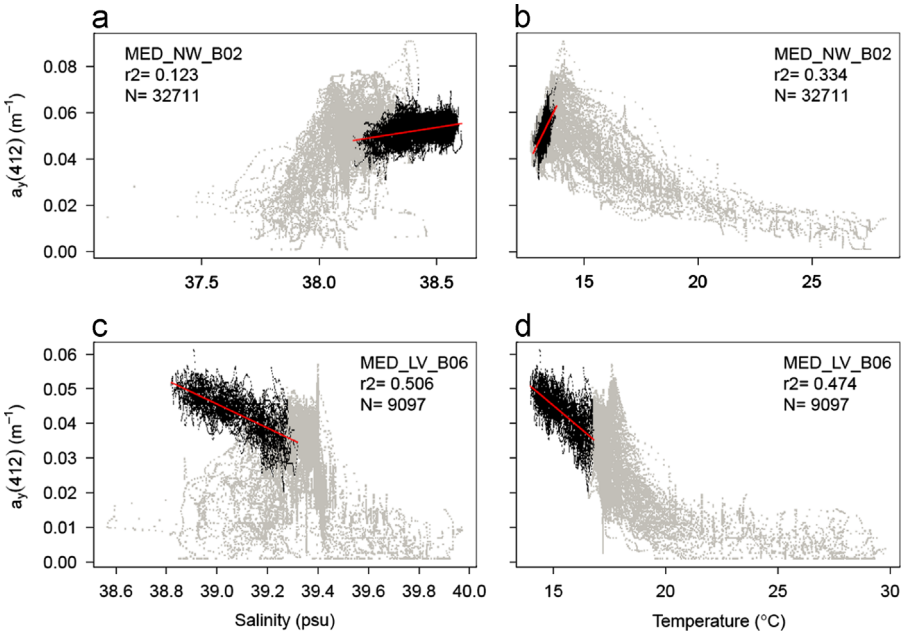

Fig. 3. The scatter plots of temperature (T, units °C) versus CDOM absorption coefficient ($a_y(412)$, units m^{-1}) (panels a and b), salinity (S, units psu) versus $a_y(412)$ (panels c and d) observed in the northwestern and eastern basin. The black points represent the measurements below the 28.88 isopycnal, and the corresponding black lines represent the best-fit regression lines with respective determination coefficients (r^2) shown in the legends.

3.4. Subsurface CDOM driven by biological activity

The 28.88 isopycnal was here used to identify the CDOM related to deep water masses, especially for the LS (see above). Similarly, the YSM is defined as the $a_y(412)$ maximum above this isopycnal. The seasonal variations of the depth of YSM (z_{YSM}) are shown in Fig. 4a and b (blue points), as well as the mixed layer depth (MLD) (black lines), the depth of deep chlorophyll-a maximum (z_{DCM}) (red lines), the penetration depth (z_{pd}) (green lines) and euphotic depth (z_{eu}) (orange lines).

The MLD exhibited the same seasonal pattern distinctly in each sub-basin. The deepest value was recorded in winter, reaching 200 m in the NWM and even exceeding 400 m in the LS, while the shallowest MLD were only 10 m in summer during the strongest stratified period. Conversely, the deepest DCM appeared in summer when the surface irradiance was maximal and subsurface chlorophyll minimal allowing a deeper penetration of photon flux. Overall, DCM became shallower in spring and autumn, and was destroyed in winter as a consequence of mixing. (Note that the red lines are discontinuous because the chlorophyll-a profile were well-mixed in winter and then DCM did not exist.) In addition, it is notable that DCM always developed close to the basis of the euphotic layer (z_{eu}).

Although the summer and fall deep CDOM was clearly evidenced from the analysis of Figs. 2c and f, there were nevertheless some outliers in the time series of z_{YSM}. For such cases, the subsurface maxima were less evident (sometimes because erratic high values were recorded at depth), especially in June and July of 2008 in the NWM, and in July and August of 2008 in the LS. The two major seasonal characteristics of subsurface CDOM remained nevertheless highly distinguishable. Firstly, the YSM was clearly located at the same depth than the DCM in fall when the former was pronounced, while z_{YSM} deepened in winter and early spring, approximately following the MLD. Especially in early winter (November and December for the NWM, January and February for the LS), the YSM did not disappear immediately as DCM with the breakdown of stratification, but descended just below the MLD and persisted for about two months more (shown in Fig. 2c and f). This revealed the detrital nature and rather refractory nature of

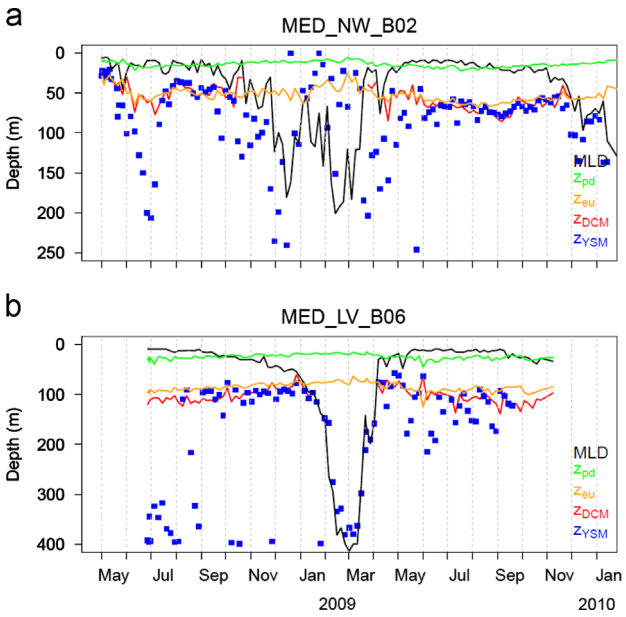

Fig. 4. The time series of the mixed layer depth (MLD, black lines), the penetration depth (z_{pd}, green lines), the euphotic depth (z_{eu}, orange lines), the depth of deep chlorophyll-a maximum (z_{DCM}, red lines) and the depth of maximal $a_y(412)$above the 28.88 isopycnal (z_{YSM}, blue points) recorded in the northwestern (a) and eastern basin (b). (For interpretation of the references to color in this figure legend, the reader is referred to the web version of this article.)

CDOM the time scales of which were evidently greater than those of Chla.

Fig. 5a and b shows the smoothed (3-point moving average) chlorophyll-a concentration at DCM and $a_y(412)$ at YSM in both sub-basins. Except for the first month in the NWM, $[Chla]_{DCM}$ generally started to increase in April, when the water column became stratified. The maximum in $[Chla]_{DCM}$ was recorded in July before a progressive decrease during late summer early fall. In parallel with the progressive decrease in processes $[Chla]_{DCM}$, $a_y(412)_{YSM}$ increased from July when phytoplankton began to decay, and persisted up to November when the decrease in [Chla]

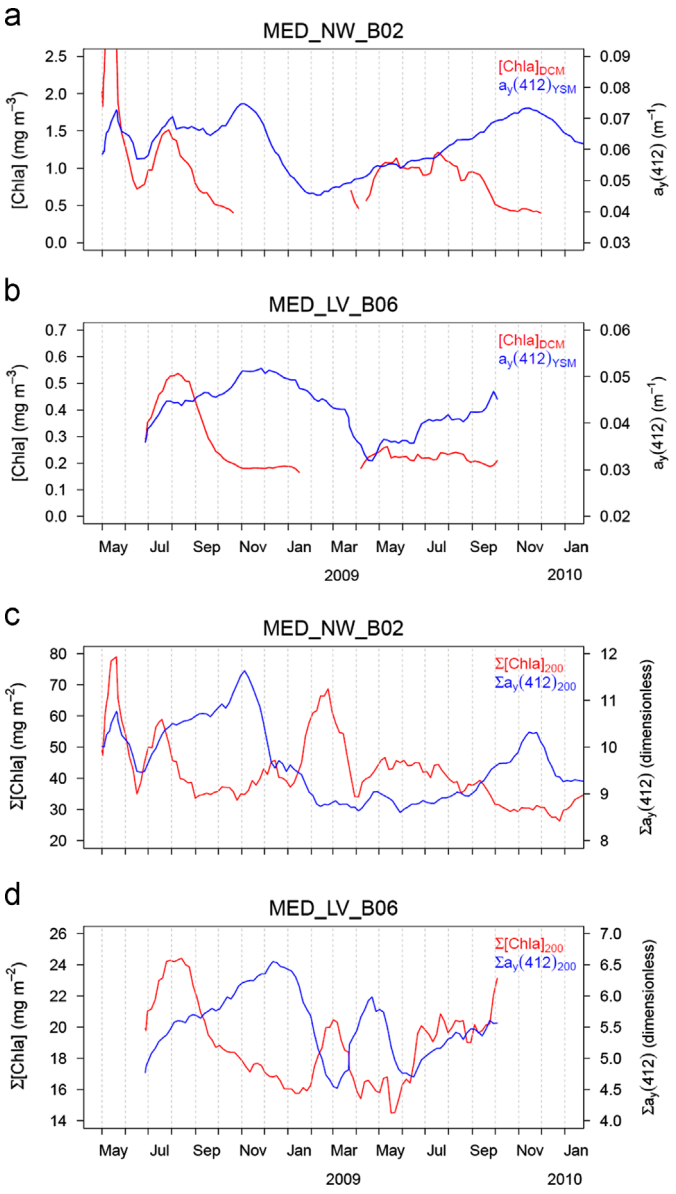

Fig. 5. Panels (a) and (b): the time series of the maximal chlorophyll-a concentration in the vertical distribution ($[Chla]_{DCM}$, red lines) and the maximal $a_y(412)$ above the 28.88 isopycnal ($a_y(412)_{YSM}$, blue lines) recorded in the northwestern (a) and eastern basin (b). Panel (c) and (d): the time series of depth-integrated chlorophyll-a concentration (red lines) and $a_y(412)$ (blue lines) from surface to 200 m in the northwestern (c) and eastern basin (d). (For interpretation of the references to color in this figure legend, the reader is referred to the web version of this article.)

stopped. This observation, together with the similar depth in YSM and DCM between July and October might suggest a tight coupling between subsurface CDOM and phytoplankton.

In order to assess the seasonal CDOM dynamics in more quantitative terms, the integrated total Chla and CDOM content ($\sum[Chla]_{200}$ and $\sum a_y(412)_{200}$) are calculated within the 0–200 m upper layer (Fig. 5c and d). Admittedly, the observed variations might be impacted by photochemical processes in surface layer (see later) but their impact was here considered as relatively minor when addressing the seasonal dynamics within this rather thick layer. It comes that this dynamics in depth-integrated chlorophyll-a and CDOM were characterized by two successive maxima: the spring maximum for Chla was the starting point of the persistent accumulation of CDOM which peaked in November for the NWM and in December for the LS, when the ML begin to destroy the DCM and to deepen the YSM.

However, in open oceans, the biogenic origin of CDOM is still a matter of debate. In general, phytoplankton was not considered as a direct source of CDOM in marine environments (e.g. via the release of exudates), but rather as a source of labile organics, which undergo microbial transformations with subsequent production of CDOM (DeGrandpre et al., 1996; Rochelle-Newall and Fisher, 2002). This viewpoint was corroborated in the Sargasso Sea, where the YSM was located at the depth of bacterial abundance maximum (BAM), but shallower than the DCM by more than 15 m (Nelson et al., 1998). Nevertheless, some other investigations reported the location of YSM at the same depth than the DCM in various regions, e.g. the Arabian Sea (Coble et al., 1998), Mid-Atlantic Bight (Chen, 1999), Baltic Sea (Lund-Hansen et al., 2006), or California Current (Chekalyuk et al., 2012). Particularly, YSM has been already found at the depth of DCM in the Mediterranean Sea, based on the measured absorption coefficients (Oubelkheir et al., 2007). These results, however, indicated that the YSM could be produced not only by bacterial activities, but also by other sources which appeared to be more phytoplankton-related.

Based on analysis of data from the Atlantic Meridional Transect, Kitidis et al. (2006) proposed the presence of two distinct CDOM end-members, characterized by different spectral dependencies. The first one was located at the DCM level and was attributed to CDOM production from phytoplankton-derived organic matter via planktonic foodweb interactions; the second one was associated with microbial remineralization. On this basis, the YSM should be interpreted as a mixture of two end-members. Besides, Oubelkheir et al. (2005) found the appearance of YSM at the depth between DCM and BAM, at one station (DYF) in the northwestern Mediterranean Sea, likely supporting the view of Kitidis et al. (2006).

Our finding in the two sub-basins of the Mediterranean Sea, however, indicated a tighter link between CDOM and phytoplankton than expected: the YSM was not only produced at the DCM level, but also followed it dynamically. When the DCM deepened in summer and shoaled in autumn (see Fig. 4a from June to November, 2009, and Fig. 4b from September to December, 2008), z_{YSM} experienced the same dynamics, which is documented for the first time thanks to the high-resolution measurements allowed by Bio-Argo floats. One plausible explanation could be that the microbial activities were closely coupled with phytoplankton, leading to the superposition of the two distinct CDOM end-members at the same depth. Another one would be that the CDOM is more associated to planktonic foodweb interactions than microbial remineralization, leading to a tighter link between YSM and DCM.

The first documented time series of CDOM dynamics by Nelson et al. (1998) in the Sargasso Sea (BATS site) highlighted that phytoplankton blooms (January–March) are followed by CDOM accumulation from the end of bloom to summer, and declined in autumn. The seasonal cycles of CDOM lagged behind the algal blooms by about 2–3 months. Similar but shorter CDOM accumulation cycles were observed in the Funka Bay, a coastal region of the Northwestern Pacific. The accumulation started in spring, rapidly reached its peak in the following first month, and then declined in summer (Sasaki et al., 2005). Differently, the CDOM cycles recorded in the Mediterranean Sea started in June when the chlorophyll-a was still increasing, and had an extended growth stage (about 5–6 months), which led to a much longer lag time between two maxima than those in the Sargasso Sea and Funka Bay.

3.5. *Surface CDOM essentially constrained by photochemical processes*

As shown in Fig., 2c and f, surface CDOM was distinctly depressed by photobleaching processes, also referred as photo-degradation or photo-oxidation. As the most important sink for

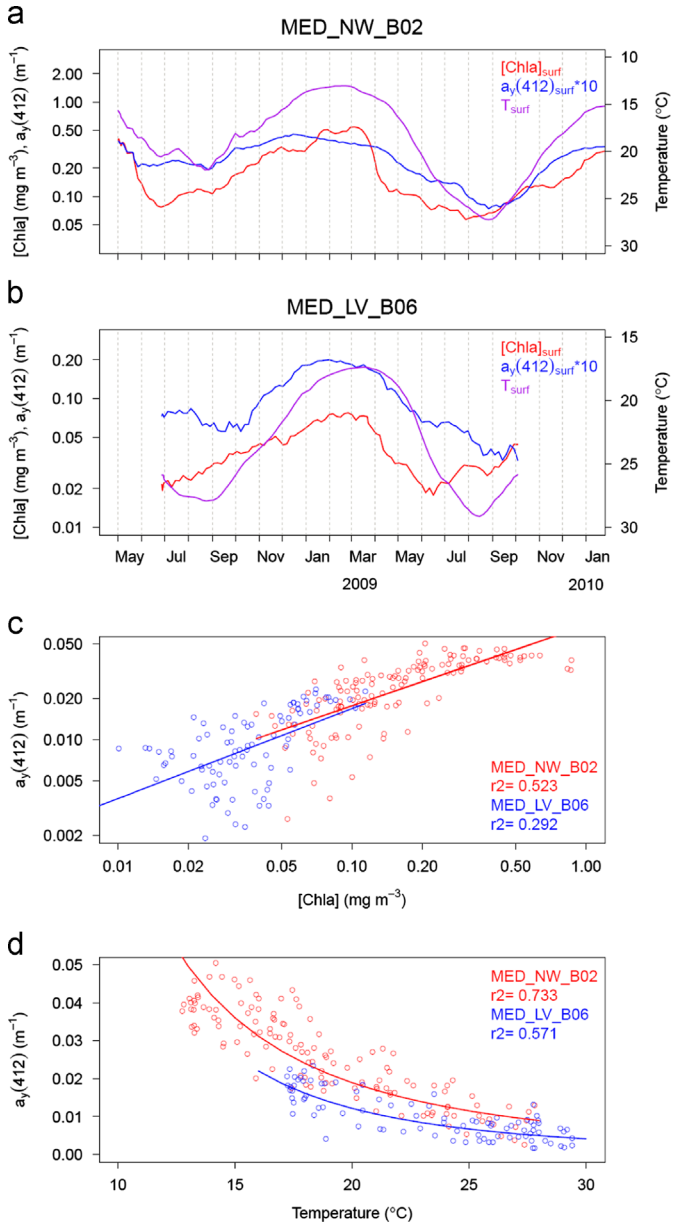

Fig. 6. The time series of surface chlorophyll-a concentration (red lines), $a_y(412)$ (blue lines) and temperature (SST purple lines) (averaged values from surface to the penetration depth) in the northwestern (a) and eastern basin (b), and their mutual relationships (c and d). The red and blue lines in the panel c and d represent the best-fit curve regressed via a power function ($y=Ax^B$) with respective determination coefficients (r^2) shown in the legends. Note that $a_y(412)$ has been exaggerated ten times for sharing the left axis with [Chla], and the right axes for temperature are reversed. (For interpretation of the references to color in this figure legend, the reader is referred to the web version of this article.)

CDOM in natural waters (Siegel and Michaels, 1996; Coble, 2007), photobleaching has been well documented in culture and in the field (Mopper et al., 1991; Kouassi and Zika, 1992; Vodacek et al., 1997; Nelson et al., 1998, 2004, 2007; Andrews et al., 2000; Whitehead et al., 2000; Yamashita and Tanoue, 2009). The dissolved inorganic carbon is considered as the major end-product of photobleaching.

To evaluate the surface CDOM dynamics and its main drivers, the averaged $a_y(412)$, [Chla] and temperature (smoothed by a 3-point moving average filter) values in z_{pd} are presented in Fig. 6a and b. In contrast to the variability at subsurface, CDOM and chlorophyll-a roughly co-varied at surface and were characterized by similar seasonal patterns, higher in winter–spring and lower in summer, which was consistent with the observation results from MODIS in the same basins (Morel and Gentili, 2009b). Despite the similar surface patterns in CDOM and chlorophyll-a, the causal mechanisms were likely different. The vertical transport of unbleached CDOM from deep waters was the main process enhancing the CDOM concentration within the upper layer. In summer, the photobleaching was mainly responsible for the depressed CDOM, while photoacclimation of intracellular chlorophyll-a concentration, together with nutrient limitation, is responsible for the lowest chlorophyll-a at surface. The scatter plots of $a_y(412)$ versus [Chla] and versus temperature (i.e. SST) are shown in Fig. 6c and d, and both correlations were examined via a power function ($y=Ax^B$). The relationships between CDOM and SST appeared more robust ($r^2=0.733$ in the NWM and 0.571 in the LS) than the one between CDOM and [Chla] ($r^2=0.523$ in the NWM and 0.292 in the LS). Furthermore, considering a larger area by analyzing, the averaged $a_{dg}(443)$ estimated by MODIS in the whole northwestern and eastern sub-basin (Fig. 7a and b) allowed to clearly confirm the seasonal patterns recorded by float. Accordingly, the relationships established from these satellite data were more robust, especially for those between CDOM and [Chla] ($r^2=0.85$ for the NWM and 0.657 for the LS). Even so, CDOM appeared to be still more dependent on SST ($r^2=0.889$ and 0.769), which were already reported at the basin and global scales (Coble et al., 1998; Nelson and Siegel, 2013). The tight inverse coupling between CDOM and SST at surface observed in situ as well as from space, implies that surface CDOM dynamics was more driven by physical processes than biological ones. Nevertheless, it does not mean that SST has a direct effect on CDOM dynamics; instead, SST is more likely a proxy of the changes in physical conditions, for instance, high SST is generally associated with increased stratification, depressed surface nutrient input, and higher average light exposure of the surface layer. These in turn are expected to impact on CDOM.

The seasonal variability of CDOM at surface thus differed quite significantly from that at subsurface (Figs. 5–7). It suggests that, therefore, the subsurface maxima and seasonal enhancement of CDOM cannot be detected at surface and by satellite data in the Mediterranean Sea, partly due to different driving mechanisms, and partly because of a relatively shallow z_{pd} (much shallower than z_{YSM}). Actually, it was truly possible to see the CDOM enhancement and time-lag effect from surface, if the YSM was sufficiently shallow compared to z_{pd} in certain regions. For example, in the central North Atlantic Ocean, the surface CDOM maxima was found in spring and lagged behind the phytoplankton bloom about 2–4 weeks based on analyses of 5 years of daily high-resolution Sea-viewing Wide Field-of-view Sensor (SeaWiFS) images (Hu et al., 2006), mainly as a result of its shallower YSM (~50 m, Nelson et al., 1998) and much deeper z_{pd} (~50 m, Hu et al., 2006) than in the Mediterranean Sea.

4. Final remarks and conclusions

Within the so-called Case I waters (Morel, 1988), CDOM and [Chla] are by principle co-varying, as CDOM is thought to be a by-product of phytoplankton. The covariant assumption allows the development of simple empirical algorithms relating ocean color to phytoplankton biomass at surface (Morel, 1988; Morel and Maritorena, 2001). As discussed above, surface CDOM dynamics would be more driven by physical processes (photobleaching), and thus partially decoupled from its phytoplankton source, even if some significant positive relationships are sometimes reported. In fact, many results suggested that there could be decoupling of CDOM and phytoplankton both globally and regionally (Siegel et al., 2002; Morel et al., 2010).

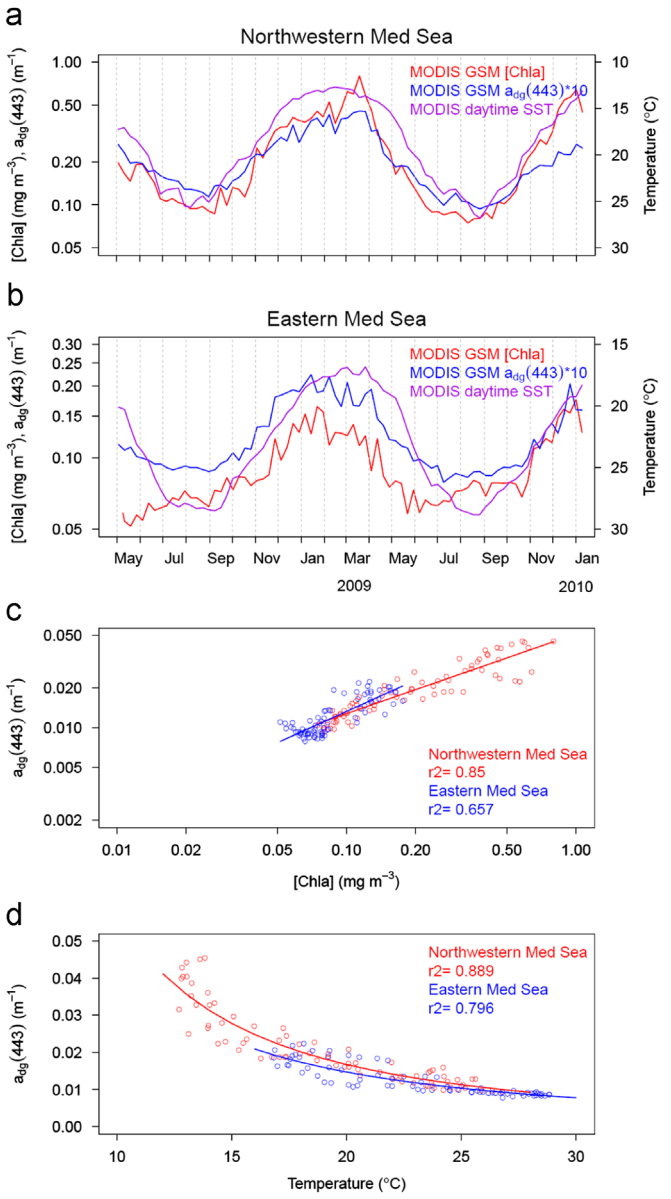

Fig. 7. The time series plots and scatter plots similar to Fig. 6, but the lines and points represent the respective averaged values in larger regions than the float trajectories observed by the MODIS satellite data (8-day composites, 9 km × 9 km resolution). The northwestern basin is chosen as 0–10°E, 39–45°N, and the eastern one as 30–37°E, 30–37°N.

In the present study, we compared the seasonal dynamics in CDOM and phytoplankton both at surface and in the upper 200 m. We found weak positive relationships within the surface layer (from 0 to z_{pd}), while the comparative dynamics at the surface appears more complicated (dephasing between both dynamics, Fig. 5a and b). Overall, there was a short positive correlation (covariance) period from spring to summer, and a long negative correlation (contravariance) period from later summer to winter. The covariance period basically corresponded to the algal growth and bloom phase. By contrast the other period corresponds to the CDOM accumulation and algal decline phase, indicating that the correlation between CDOM and phytoplankton in the euphotic layer depended on the phytoplankton physiological status. Although many studies reported that in situ production of CDOM was not directly derived from phytoplankton itself, our finding in the Mediterranean Sea suggested that there existed a tight but indirect coupling between CDOM and phytoplankton via other intermediate processes.

Apart from river inputs and upwelling of deep waters, there are two main sources of CDOM in subsurface layers, microbial activity and planktonic foodweb interactions (Coble, 2007). In the global ocean, CDOM was found ubiquitously related to inorganic nutrient distribution and apparent oxygen utilization, suggesting a link between microbial remineralization and CDOM (Chen and Bada, 1992; Hayase and Shinozuka, 1995; Jørgensen et al., 2011). Most apparently in the Sargasso Sea, the YSM was recorded around 50 m depth, typically shallower than the DCM layer (90–120 m), but agreed with the depth of the highest bacteria biomass and productivity in the upper water column (Nelson et al., 1998). It was thus concluded that the microbial community is the source of the "new" summer time CDOM. However, the phytoplankton-related CDOM was also identified in some regions, generally characterized by appearance of YSM at the same depth than the DCM (Coble et al., 1998; Chen, 1999; Lund-Hansen et al., 2006; Kitidis et al., 2006; Oubelkheir et al., 2007; Chekalyuk et al., 2012).

Therefore, the subsurface maxima and seasonal cycles in CDOM and phytoplankton observed here could likely be the result of either microbial processes or plankton trophic relationships. At this point, these observations cannot be further confirmed here because of the lack of concomitant observations of other ancillary parameters (such as bacterial production, nutrient level and/or apparent oxygen utilization).

There are now Bio-Argo floats with multi-sensor package (e.g. including bio-optics, oxygen, nitrate, etc.). Similarly there is sensor development to possibly measure zooplankton biomass from floats and or gliders. These new multi-instrumented platforms will likely contribute to a further understanding of CDOM seasonal dynamics and associated underlying mechanisms both at regional and global scales.

Acknowledgments

This paper represents a contribution to the remOcean (REMotely sensed biogeochemical cycles in the OCEAN, GA 246777) project funded by the European Research Council, to the Plateformes Autonomes et Biogéochimie Océanique (PABO) project, funded by Agence Nationale de la Recherche, to the China Postdoctoral Science Foundation funded project (2012M511547), to the National Natural Science Foundation of China (41206028, 41076114, 41023007), to the Public Science and Technology Research Funds Projects of Ocean (201005030), and to the MEL Visiting Fellowship Program (MELRS1220).

References

Andrews, S.S., Caron, S., Zafiriou, O.C., 2000. Photochemical oxygen consumption in marine waters: a major sink for colored dissolved organic matter? Limnology and Oceanography 45, 267–277.
Belzile, C., Roesler, C.S., Christensen, J.P., Shakhova, N., Semiletov, I., 2006. Fluorescence measured using the WETStar DOM fluorometer as a proxy for dissolved matter absorption. Estuarine, Coastal and Shelf Science 67, 441–449.
Chekalyuk, A.M., Landry, M.R., Goericke, R., Taylor, A.G., Hafez, M.A., 2012. Laser fluorescence analysis of phytoplankton across a frontal zone in the California Current ecosystem. Journal of Plankton Research 34, 761–777.
Chen, R.F., 1999. In situ fluorescence measurements in coastal waters. Organic Geochemistry 30, 397–409.
Chen, R.F., Bada, J.L., 1992. The fluorescence of dissolved organic matter in seawater. Marine Chemistry 37, 191–221.
Claustre, H., Bishop, J., Boss, E., Stewart, B., Berthon, J.-F., Coatanoan, C., Johnson, K., Lotiker, A., Ulloa, O., Perry, M.-J., D'Ortenzio, F., Hembise Fanton D'Andon, O., Uitz, J., 2010. Bio-optical profiling floats as new observational tools for biogeochemical and ecosystem studies: potential synergies with ocean color remote sensing. In: Hall, J., Harrison, D.E., Stammer, D. (Eds.), Proceedings of OceanObs'09: Sustained Ocean Observations and Information for Society, vol. 2.

ESA Publication WPP-306, Venice, Italy,http://dx.doi.org/10.5270/OceanObs09.cwp.17 (21–25 September 2009).
Coble, P.G., 1996. Characterization of marine and terrestrial DOM inseawater using excitation–emission matrix spectroscopy. Marine Chemistry 51, 325–346.
Coble, P.G., 2007. Marine optical biogeochemistry: the chemistry of ocean color. Chemical Reviews 107, 402–418.
Coble, P.G., Del Castillo, C.E., Avril, B., 1998. Distribution and optical properties of CDOM in the Arabian Sea during the 1995 southwest monsoon. Deep-Sea Research, Part II 45, 2195–2223.
De Boyer Montégut, C., Madec, G., Fischer, A.S., Lazar, A., Iudicone, D., 2004. Mixedlayer depth over the global ocean: an examination of profile data and a profile-basedclimatology. Journal of Geophysical Research 109, C12003.
DeGrandpre, M.D., Vodacek, A., Nelson, R.K., Bruce, E.J., Blough, N.V., 1996. Seasonal seawater optical properties of the US Middle Atlantic Bight. Journal of Geophysical Research 101C, 22727–22736.
De Souza Sierra, M.M., Donard, O.F.X., Lamotte, M., 1997. Spectral identification and behavior of dissolved organic fluorescent material during estuarine mixing processes. Marine Chemistry 58, 51–58.
Ferrari, G.M., 2000. The relationship between chromophoric dissolved organic matter and dissolved organic carbon in the European Atlantic coastal area and in the West Mediterranean Sea (Gulf of Lions). Marine Chemistry. 70, 339–357.
Ferrari, G., Dowell, M.D., 1998. CDOM absorption characteristics with relation to fluorescence and salinity in coastal areas of the southern Baltic Sea. Estuarine, Coastal and Shelf Science 47, 91–105.
Ferrari, G., Tassan, S., 1991. On the accuracy of determining light absorption by “yellow substance” through measurements of induced fluorescence. Limnology and Oceanography 36, 777–786.
Fusco, G., Manzella, G.M.R., Cruzado, A., Gačić, M., Gasparini, G.P., Kovačević, V., Millot, C., Tziavos, C., Velasquez, Z.R., Walne, A., Zervakis, V., Zodiatis, G., 2003. Variability of mesoscale features in the Mediterranean Sea from XBT data analysis. Annales Geophysicae 21, 21–32.
Hayase, K., Shinozuka, N., 1995. Vertical distribution of fluorescent organic matter along with AOU and nutrients in the equatorial Central Pacific. Marine Chemistry 48, 283–290.
Herbaut, C., Mortier, L., Crépon, M., 1996. A sensitivity study ofthe general circulation of the Western Mediterranean Sea. Journal of Physical Oceanography 26, 65–84.
Hoge, F.E., Swift, R.N., Yungel, J.K., Vodacek, A., 1993. Fluorescence of dissolved organic matter: a comparison of North Pacific and North Atlantic Oceans during April 1993. Journal of Geophysical Research 98 (C12), 22779–22787.
Hu, C., Lee, Z., Muller-Karger, F.E., Carder, K.L., Walsh, J.J., 2006. Ocean color reveals phase shift between marine plants and yellow substance. IEEE Geoscience and Remote Sensing Letters 3, 262–266.
IOCCG, 2011. Bio-optical sensors on argo floats. In: Claustre, H. (Ed.), Reports of the International Ocean-Color Coordinating Group, No. 11. Darthmouth, Canada.
Johnson, K.S., Berelson, W.M., Boss, E.S., Chase, Z., Claustre, H., Emerson, S.R., Gruber, N., Körtzinger, A., Perry, M.J., Riser, S.C., 2009. Observing biogeochemical cycles at global scales with profiling floats and gliders: prospects for a global array. Oceanography 22, 216–225.
Jørgensen, L., Stedmon, C.A., Kragh, T., Markager, S., Middelboe, M., Søndergaard, M., 2011. Global trends in the fluorescence characteristics and distribution of marine dissolved organic matter. Marine Chemistry 126, 139–148.
Kalle, K., 1938. Zum problem der meerwasserfarbe. Annalen der Hydrologischen und Marinen Mitteilungen 66, 1–13.
Kalle, K., 1949. Fluoreszenz und Gelbstoff im Bottnischen und Finnischen Meerbusen. Deutsche Hydrographische Zeitschrift. 2, 117–124.
Kirk, J.T.O., 1994. Light and Photosynthesis in Aquatic Ecosystems, 2nd ed. Cambridge University Press, Cambridge.
Kitidis, V., Stubbins, A.P., Uher, G., Upstill Goddard, R.C., Law, C.S., Woodward, E.M. S., 2006. Variability of chromophoric organic matter in surface waters of the Atlantic Ocean. Deep-Sea Research, Part II 53, 1666–1684.
Kouassi, A.M., Zika, R.G., 1992. Light-induced destruction of the absorbance property of dissolved organic matter in seawater. Toxicological & Environmental Chemistry 35, 195–211.
Kowalczuk, P., Zablocka, M., Sagan, S., Kulinski, K., 2010. Fluorescence measured in situ as a proxy of CDOM absorption and DOC concentration in the Baltic Sea. Oceanologia 52, 431–471.
Laane, R.W.P.M., Kramer, K.J.M., 1990. Natural fluorescence in the North Sea and its major estuaries. Netherlands Journal of Sea Research 26, 1–9.
Lund-Hansen, L.C., De Amezua Ayala, P.C., Reglero, A.F., 2006. Bio-optical properties and development of a sub-surface chlorophyll maxima (SCM) in southwest Kattegat, Baltic Sea. Estuarine, Coastal and Shelf Science 68, 372–378.
Maritorena, S., Siegel, D.A., Peterson, A.R., 2002. Optimization of a semianalytical ocean color model for global-scale applications. Applied Optics 41, 2705–2714.
Mopper, K., Schultz, C.A., 1993. Fluorescence as a possible tool for studying the nature and water columndistribution of DOC components. Marine Chemistry 41, 229–238.
Mopper, K., Zhou, X.L., Kieber, R.J., Kieber, D.J., Sikorski, R.J., Jones, R.D., 1991. Photochemical degradation of dissolved organic carbon and its impact on the oceanic carbon cycle. Nature 353, 60–62.
Morel, A., 1988. Optical modeling of the upper ocean in relation to its biogenous matter content (Case I waters). Journal of Geophysical Research 93, 10749–10768.
Morel, A., Gentili, B., 2009a. A simple band ratio technique to quantify the colored dissolved and detrital organic material from ocean color remotely sensed data. Remote Sensing of Environment 113, 998–1011.
Morel, A., Gentili, B., 2009b. The dissolved yellow substance and the shades of blue in the Mediterranean Sea. Biogeosciences 6, 2625–2636.
Morel, A., Maritorena, S., 2001. Bio-optical properties of oceanic waters: a reappraisal. Journal of Geophysical Research 106, 7163–7180.
Morel, A., Huot, Y., Gentili, B., Werdell, P.J., Hooker, S.B., Franz, B.A., 2007. Examining the consistency of products derived from various ocean color sensors in open ocean (Case 1) waters in the perspective of a multi-sensor approach. Remote Sensing of Environment 111, 69–88.
Morel, A., Claustre, H., Gentili, B., 2010. The most oligotrophic subtropical zones of the global ocean: similarities and differences in terms of chlorophyll and yellow substance. Biogeosciences 7, 3139–3151.
Nelson, N.B., Siegel, D.A., 2002. Chromophoric DOM in the open ocean. In: Hansell, D.A., Carlson, C.A. (Eds.), Biogeochemistry of Marine Dissolved Organic Matter. Academic Press, San Diego, CA, pp. 547–578.
Nelson, N.B., Siegel, D.A., 2013. The global distribution and dynamics of chromophoricdissolved organic matter. Annual Review of Marine Science 5, 447–476.
Nelson, N.B., Siegel, D.A., Michaels, A.F., 1998. Seasonal dynamics of colored dissolved material in the Sargasso Sea. Deep-Sea Research, Part I 45, 931–957.
Nelson, N.B., Carlson, C.A., Steinberg, D.K., 2004. Production of chromophoric dissolved organic matter by Sargasso Sea microbes. Marine Chemistry 89, 273–287.
Nelson, N.B., Siegel, D.A., Carlson, C.A., Swan, C., Smethie Jr., W.M., Khatiwala, S., 2007. Hydrography of chromophoric dissolved organic matter in the North Atlantic. Deep-Sea Research, Part I 54, 710–731.
Oubelkheir, K., Claustre, H., Babin, M., Sciandra, A., 2005. The comparative bio-optical and biogeochemical properties of contrasted trophic regimes. Limnology and Oceanography 50, 1795–1809.
Oubelkheir, K., Claustre, H., Bricaud, A., Babin, M., 2007. Partitioning total spectral absorption in phytoplankton and coloreddetrital material contribution. Limnology and Oceanography: Methods 5, 384–395.
Rochelle-Newall, E.J., Fisher, T.R., 2002. Production of chromophoric dissolved organic matter fluorescence in marine andestuarine environments: an investigation into the role of phytoplankton. Marine Chemistry 77, 7–21.
Sasaki, H., Miyamura, T., Saitoh, S., Ishizaka, J., 2005. Seasonal variation of absorption by particles and colored dissolved organic matter (CDOM) in Funka Bay, southwestern Hokkaido, Japan. Estuarine, Coastal and Shelf Science 64, 447–458.
Shifrin, K.S., 1988. Physical Optics of Ocean Water. In: Oliver, D. (Ed.), 1988. American Institute of Physics, New York.
Siegel, D.A., Michaels, A.F., 1996. Non-chlorophyll light attenuation in the open ocean: implications for biogeochemistry and remote sensing. Deep-Sea Research, Part II 43, 321–345.
Siegel, D.A., Michaels, A.F., Sorensen, J.C., O'Brien, M., Hammer, M.A., 1995. Seasonal variability of light availability and utilization in the Sargasso Sea. Journal of Geophysical Research 100, 8675–8713.
Siegel, D.A., Maritorena, S., Nelson, N.B., Hansell, D.A., Lorenzi-Kayser, M., 2002. Global distribution and dynamics of colored dissolved and detrital organic materials. Journal of Geophysical Research 107, 3228.
Swan, C.M., Siegel, D.A., Nelson, N.B., Carlson, C.A., Nasir, E., 2009. Biogeochemical and hydrographic controls on chromophoric dissolved organic matter distribution in the Pacific Ocean. Deep-Sea Research, Part I 56, 2175–2192.
Vodacek, A., Blough, N.V., DeGrandpre, M.D., Peltzer, E.T., Nelson, R.K., 1997. Seasonal variation of CDOM and DOC in the Middle Atlantic Bight: terrestrial inputs and photooxidation. Limnology and Oceanography 42, 674–686.
Whitehead, R.R., De Mora, S., Demers, S., Gosselin, M., Monfort, R., Mostajir, B., 2000. Interactions of ultraviolet-B radiation, mixing, and biological activity on photobleaching of natural chromophoric dissolved organic matter: a mesocosm study. Limnology and Oceanography 45, 278–291.
Xing, X., Morel, A., Claustre, H., Antoine, D., D'Ortenzio, F., Poteau, A., Mignot, A., 2011. Combined processing and mutual interpretation of radiometry and fluorimetry from autonomous profiling Bio-Argo Floats: chlorophyll a retrieval. Journal of Geophysical Research 116, C06020.
Xing, X., Morel, A., Claustre, H., Antoine, D., D'Ortenzio, F., Poteau, A., 2012. Combined processing and mutual interpretation of radiometry and fluorometry from autonomous profiling Bio-Argo floats: 2. Colored dissolved organic matter absorption retrieval. Journal of Geophysical Research 117, C04022.
Yamashita, Y., Tanoue, E., 2009. Basin scale distribution of chromophoric dissolved organic matter in the Pacific Ocean. Limnology and Oceanography 54, 598–609.